Applied Catalysis B: Environmental 158–159 (2014) 341–347

Contents lists available at ScienceDirect

Applied Catalysis B: Environmental

journal homepage: www.elsevier.com/locate/apcatb

Highly efficient mesoporous Pd/CeO_2 catalyst for low temperature CO oxidation especially under moisture condition

Gengnan Li [a], Liang Li [a,*], Yuan Yuan [a], Jingjing Shi [a], Yinyin Yuan [a], Yongsheng Li [a], Wenru Zhao [a], Jianlin Shi [a,b]

[a] Key Laboratory for Ultrafine Materials of Ministry of Education, School of Materials Science and Engineering, East China University of Science and Technology, Shanghai 200237, China
[b] State Key Laboratory of High Performance Ceramic and Superfine Microstructure, Shanghai Institute of Ceramics, Chinese Academy of Sciences, Shanghai 200050, China

ARTICLE INFO

Article history:
Received 10 January 2014
Received in revised form 10 March 2014
Accepted 16 April 2014
Available online 24 April 2014

Keywords:
Mesoporous catalyst
Heterogeneous catalysis
CO oxidation
Cerium oxide

ABSTRACT

The Pd/CeO_2 catalyst was successfully prepared by an improved impregnation protocol. The resulting materials possessed relatively high specific surface area and highly dispersed Pd nanoparticles. For low temperature CO oxidation reaction, 2.5 wt% Pd loaded catalyst showed the much higher reaction activity. The total conversion temperature was as low as 40 °C under dry condition, much lower than that synthesized by other method. More importantly, the material also showed excellent catalytic activity and stability under moisture condition. When 2.5 vol% H_2O was introduced into the feed gas, the catalytic activity showed significantly enhancement, the CO total conversion temperature decreased from 40 °C to 30 °C. The catalytic mechanism and reaction kinetic study were also discussed in detail.

1. Introduction

Ceria-supported noble metal catalysts have received considerable attention in recent years, mainly due to their applications in oxidation of hydrocarbon, carbon monoxide and other harmful gases discharged by automotive emissions [1–9]. Among them, the palladium contained cerium oxide catalyst is notable for its high activity, successful oxidation of CO at low temperature, and high stability over a wide range of temperature [10]. It is generally recognized that the unique performance of this catalyst is determined not only by the active component (palladium) but also the interaction between palladium and cerium oxide matrix [7,8,10–13]. The deposition of palladium could stimulate the mobility of lattice oxygen at the interface between noble metal and support, and meanwhile retain the oxygen storage capacity of CeO_2, which can significantly promote the catalytic activity of CO oxidation [10,14–16]. Thus, the geometric structure of CeO_2 support and the dispersion of palladium nanoparticles are key factors for highly efficient Pd/CeO_2 catalyst for low temperature CO oxidation.

On the other hand, the fundamental studies about Pd/CeO_2 catalyst for CO oxidation so far are usually carried out under dry condition. However, moisture is inevitably existed in practical applications especially for low temperature oxidation and plays a completely different role in the presence/absence of noble metals [17,18]. It could be a devastatingly poisonous species for transition metal oxide or a promoter for noble metal [17,19,20]. Thus, it is more important to study the catalytic behavior of CO oxidation under moisture condition. Up to date, although many catalytic systems have been developed, low temperature CO oxidation catalyst for practical applications under moisture condition is still expected and in challenge [17–19].

In this work, mesoporous CeO_2 support was fabricated through pyrolysis of oxalate and palladium was loaded by an improved wet impregnation and in situ reduction protocol. Oxalate was chosen as the precursor for pyrolysis mainly due to its easy synthesis, low cost, good structure stability and relatively low decomposition temperature in air. The resulting metal oxide possessed mesoporous structure and high specific surface area, which were suitable for loading noble metals [21]. In addition, the improved wet impregnation method was a useful way of introducing the specific components into the porous structure. After impregnation, the noble metal ion species could transform into metal oxide, and the noble metal nanoparticles were in situ produced directly by using hydrazine hydrate as reductant, subsequently. Compared with the traditional impregnation method [11], this strategy was simple and time-saving. The resulting materials owned high surface area and the palladium nanoparticles could be homogeneously deposited in/on the CeO_2 support, and thus possessed the much higher catalytic activities. The water resistance of the resulting

* Corresponding author. Tel.: +86 021 64252599; fax: +86 021 64250740.
E-mail address: liliang@ecust.edu.cn (L. Li).

http://dx.doi.org/10.1016/j.apcatb.2014.04.030
0926-3373/

Pd/CeO_2 material, catalytic mechanism and reaction kinetic study were also discussed in detail.

2. Experimental

2.1. Materials preparation

10 mmol $Ce(NO_3)_2{\cdot}6H_2O$ was dissolved into 100 ml aqueous solution, then 30 ml 1 M oxalate was slowly added under vigorous stirring. The precipitate was filtered, washed with deionized water and dried at 60 °C. The mesporous CeO_2 material was finally obtained after calcinated at 350 °C for 2 h.

A series of mesoporous CeO_2 supported Pd catalysts were synthesized through an improved wet impregnation procedure. In a typical synthesis, 0.5 g mesoporous CeO_2 material was added in 25 ml aqueous solution containing calculated content of Na_2PdCl_4, After stirred for 2 h, 100 ml 0.1 M hydrazine hydrate ($NH_2{\cdot}NH_2{\cdot}H_2O$) was slowly added and stirred for 12 h successively. The resulting solid mass was collected through centrifugation, washed with water and dried at 60 °C for 24 h.

2.2. Characterization

Powder X-ray diffraction (XRD) patterns were recorded on a Bruker D8 Focus powder diffract meter with graphite mono chromatized Cu Kα radiation (λ = 0.15405 nm) operated at 40 kV. Thermo gravimetric analysis (TG–DSC) were carried out at a heating rate of 10 °C/min from ambient temperature to 700 °C with an air flow rate of 20 ml min^{-1}. Nitrogen adsorption and desorption isotherms were measured on a Micromeritics ASAP 2020M analyzer at liquid nitrogen temperature (77 K). Prior to the measurements, the samples were degassed at 423 K in vacuum for 6 h. The specific surface area and pore size distribution were calculated using the Brunauer–Emmett–Teller (BET) and Barrett–Joyner–Halenda (BJH) methods, respectively. Transmission Electron Microscopy (TEM) observations were performed on a field emission JEM-2100 (JEOL) electron microscope operated at 300 kV equipped with a Gatan-666 electron energy loss spectrometer and energy dispersive X-ray spectrometer. XPS (X-ray photoelectron spectroscopy) signals were collected on a VG Micro MK II instrument using monochromatic Al Kα X-ray at 1486.6 eV operated at 200 W. All the elemental binding energies were referenced to the C (1s) line situated at 284.6 eV.

2.3. CO oxidation test

The catalytic test for CO oxidation was carried out in fixed-bed quartz tubular reactor (i.d. = 6 mm) containing 200 mg of catalyst samples without any pretreatment. A standard reaction gas contained 1.0 vol% CO, 20.0 vol% O_2 and high-purity N_2 (99.99%) gas was used as sources to form desired gas mixture. The feed gas at a flow rate of 50 ml min^{-1} was introduced into the reactor using mass-flow controllers, corresponding to a space velocity of 15,000 ml h^{-1} $g_{cat}{}^{-1}$. After the steady operation for 10 min, the activity of catalyst was tested. The conversion of CO was measured by online gas chromatograph (GC) equipped with a FID under steady-state conditions. The reaction temperature was monitored by a thermocouple placed in the middle of the catalyst bed. The activity of the catalyst in the presence of moisture condition was tested by passing the feed gas at a flow rate of 50 ml min^{-1} through a water vapor saturator. Changing the temperature of saturator can adjust the water concentration in the feed gas.

2.4. Reaction kinetics

The kinetic study was performed on the same fixed bed reactor. The reactor was operated in a differential mode with CO conversion less than 15%. The reactant gas consisted of 1.0% CO, 20.0% O_2, 2.5% H_2O balanced with N_2. The reaction rates were obtained after the reaction run for 30 min.

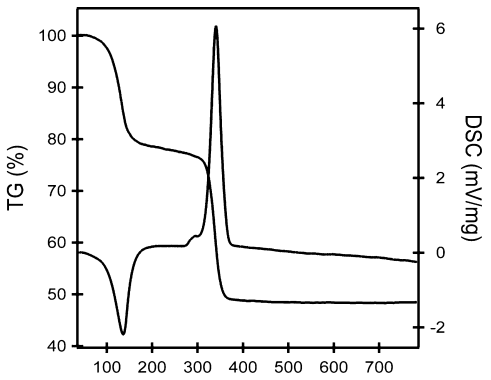

Fig. 1. The TG–DSC curves of the $Ce_2(C_2O_4)_3{\cdot}8H_2O$ precursor.

3. Results and discussion

Mesoporous CeO_2 support was fabricated through pyrolysis of oxalate. The thermal behavior of the oxalate precursor was firstly investigated by TG–DSC analysis in a static air atmosphere at a heating rate of 10 °C/min, as presented in Fig. 1. During the calcination, the oxalate precursor lost 52% of its original weight in two steps accompanied by an endothermic and an exothermic process, as shown in the DSC line. The endothermic event occurs at about 137 °C, corresponding to the elimination of the coordinated water. With the increasing of temperature, there is a rapid change in mass loss in the TG curve, suggesting the decomposition of oxalate groups and oxidation of the precursor into crystalline CeO_2. This stage appears a strong exothermic peak around 330 °C in the DSC curve. The weight residual becomes constant when temperature rises to about 350 °C.

The crystalline structure of oxalate precursor and resulting Pd/CeO_2 materials were then characterized by X-ray diffraction (XRD) analysis. Fig. 2A depicts XRD pattern of the oxalate precursor, which agrees well with the crystalline $Ce_2(C_2O_4)_3{\cdot}8H_2O$ (PDF card No. 20-0268). After calcined at 350 °C for 2 h, the precursor lost its original crystalline structure and turned to CeO_2 (PDF card No. 81-0792). No additional diffraction peaks from impurities were detected. Sequential impregnation and in situ reduction process did not affect the crystalline structure of the CeO_2 support. Fig. 2B presents the XRD patterns of the obtained Pd/CeO_2 catalysts with different Pd loading content. Except that for CeO_2 support, a peak emerged at $2\theta = 40°$ which can be identified as (1 1 1) diffraction band of face-centered cubic structure palladium. The diffraction intensity increases with the increase of loaded Pd content. It should be note that all the characteristic peaks of metallic Pd are broadened and weak indicating the highly dispersed amorphous or small palladium nanoparticles. The actual contents of Pd in the mesostructured Pd/CeO_2 materials were determined by the ICP-AES technique to be 1.1%, 2.5%, 5.1%, 9.6%, Although the loaded contents were somewhat lower than the initial values, the most of the Pd in the aqueous solution have been deposited into or on the mesoporous CeO_2 support.

The Transmission Electron Microscopy (TEM) analysis was employed to examine the morphology and Pd distribution of the materials (Fig. 3). Thanks to the slow heating program (1 °C/min), the CeO_2 support possesses porous structure with sponge-like pore network randomly but homogeneously distributed within the whole particles [22]. Rapid heating of sample could cause the violent gas evolution, leading to the remarkable shrinkage

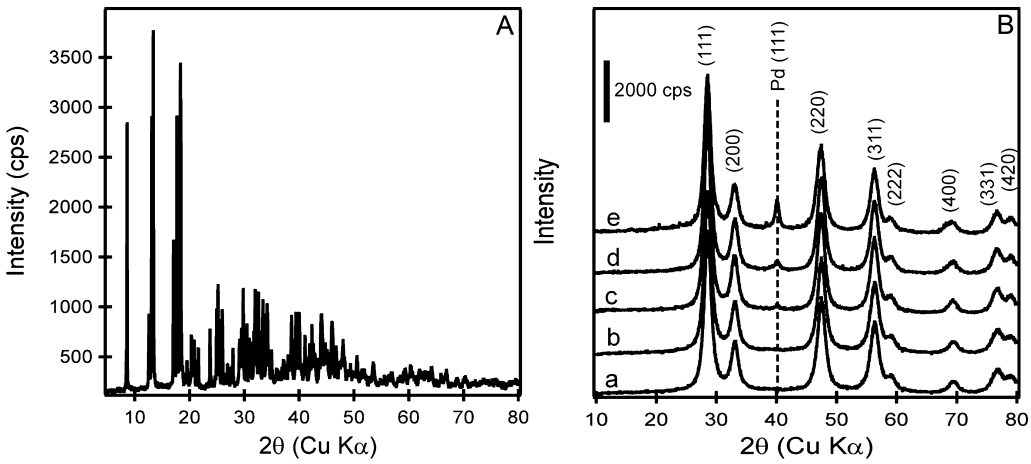

Fig. 2. TheXRD patterns of $Ce_2(C_2O_4)_3{\cdot}8H_2O$ precursor (A) and Pd/CeO_2 catalysts with different Pd loading contents (B): 0 wt% (a), 1.1 wt% (b), 2.5 wt% (c), 5.1 wt% (d), 9.6 wt% (e).

and disruption of the block morphology. During the thermal process, the decomposition of oxalate particles leaves numerous voids behind, forming mesoporous structure. After impregnation, the noble metal ion species $PdCl_4^{2-}$ transform into metal oxide. The following in situ reduction process results in Pd/CeO_2 material with Pd nanoparticles being homogeneously dispersed in/on the mesoporous support. In addition, the Selected Area Electron Diffraction (SAED) patterns from the same area are also presented in the images. The well-defined diffraction rings for CeO_2 can be found in all the samples. However, the relative faint diffraction rings of palladium indicate its much lower crystallinity. These results are in good agreement with above XRD analysis. From the High Resolution Transmission Electron Microscopy (HRTEM) investigation (Fig. 3F), the (1 1 1) plane of metallic Pd can be clearly distinguished. The average particle sizes collected from over 10 different particles is about 5 nm in diameter independent of the deposition amount.

After loaded with palladium, the materials still possess mesoporous structure. Impregnation and in situ reduction process did not affect the meso-structured nature of the CeO_2 support, as confirmed by the adsorption-desorption isotherms of nitrogen at 77 K (Fig. 4). In all the cases, the typical Langmuir IV isotherms suggest the mesoporous structure and the appearance of H3 hysteresis loops indicate the formation of slit-like mesopore. It is noticeable that the specific surface area and pore size of the samples show only limited change with the increase of palladium loading amount. These results demonstrate that palladium nanoparticles have been uniformly dispersed and ungrowth during the deposition, corresponding well with the above XRD and TEM analysis.

The surface chemical states of the species for Pd/CeO_2 catalysts were detected by X-ray photoelectron spectroscopy (XPS). Fig. 5A depicts the Ce 3d XPS spectra of Pd/CeO_2 materials (the related binding energy of different chemical states are listed in Table 1). Generally, the Ce 3d spectrum is somewhat complicated and composed with two series of peaks: $3d_{5/2}$ with two very pronounced "shake-down" satellites and $3d_{3/2}$ with the same characteristics (Table 2) [10,23]. It can be found that both of Ce^{4+} and Ce^{3+} exist abundantly in all the Pd/CeO_2 materials, which indicate not fully oxidized surface of the samples. It can be inferred that the oxygen vacancies are always presented in Pd/CeO_2 catalysts. Accordingly, promote the oxygen release and store during the CO oxidation process. In addition, the percentage of Ce^{3+} decrease with the increasing of Pd content, which could directly affect the catalytic performance for CO oxidation. The O 1s XPS spectra of the catalysts can be resolved into two peaks as shown in Fig. 5B. The main contribution at 529.5 eV is the characteristic peak of metal–oxygen due to the lattice oxygen, and that at 531.5 eV is usually associated with the surface adsorbed oxygen (chemisorbed oxygen) [24]. With the increase of Pd loading amount, the amount of absorbed oxygen

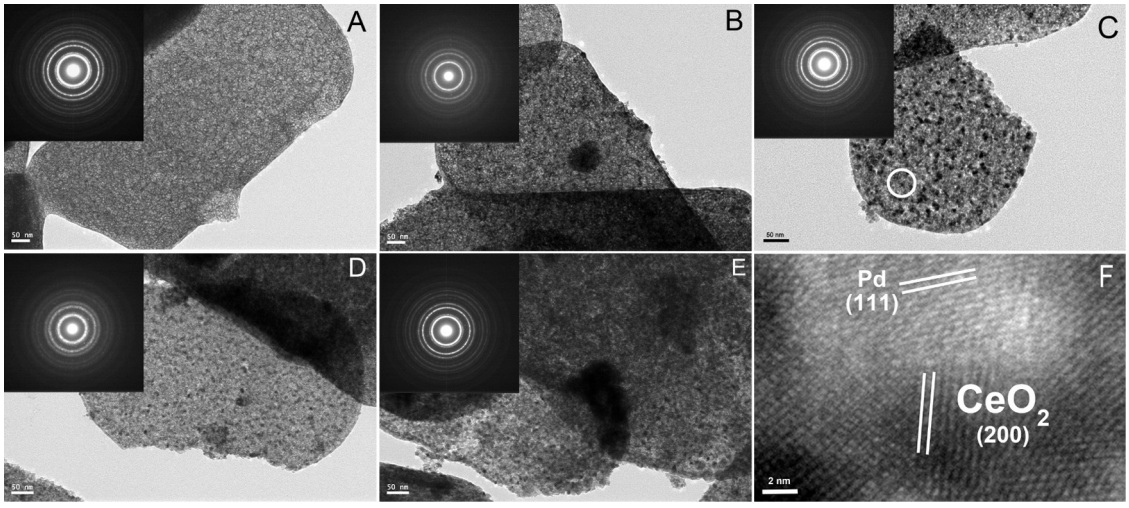

Fig. 3. The TEM and HRTEM images of the CeO_2 support (A) and Pd/CeO_2 catalysts with different Pd loading contents: 1.1 wt% (B), 2.5 wt% (C and F), 5.1 wt% (D), 9.6 wt% (E).

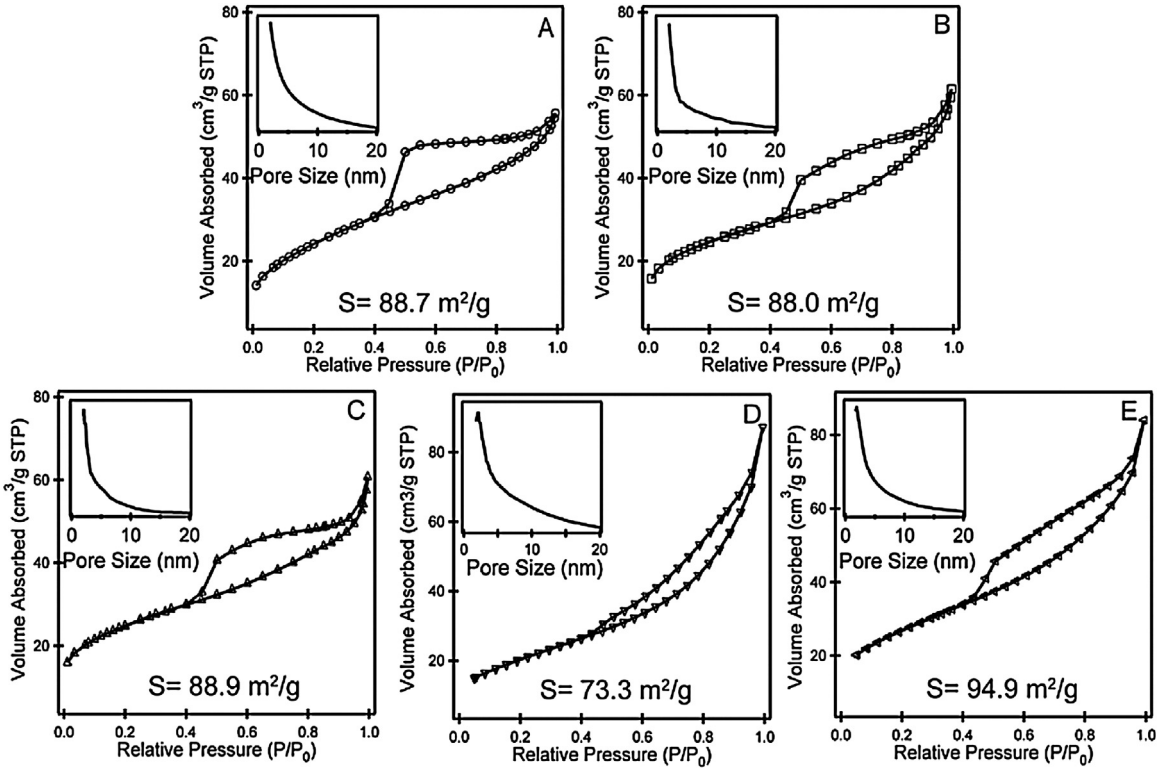

Fig. 4. The N_2 adsorption-desorption analysis of the CeO_2 support (A) and the Pd/CeO_2 catalysts with different Pd loading contents: 1.1 wt% (B), 2.5 wt% (C), 5.1 wt% (D), 9.6 wt% (E).

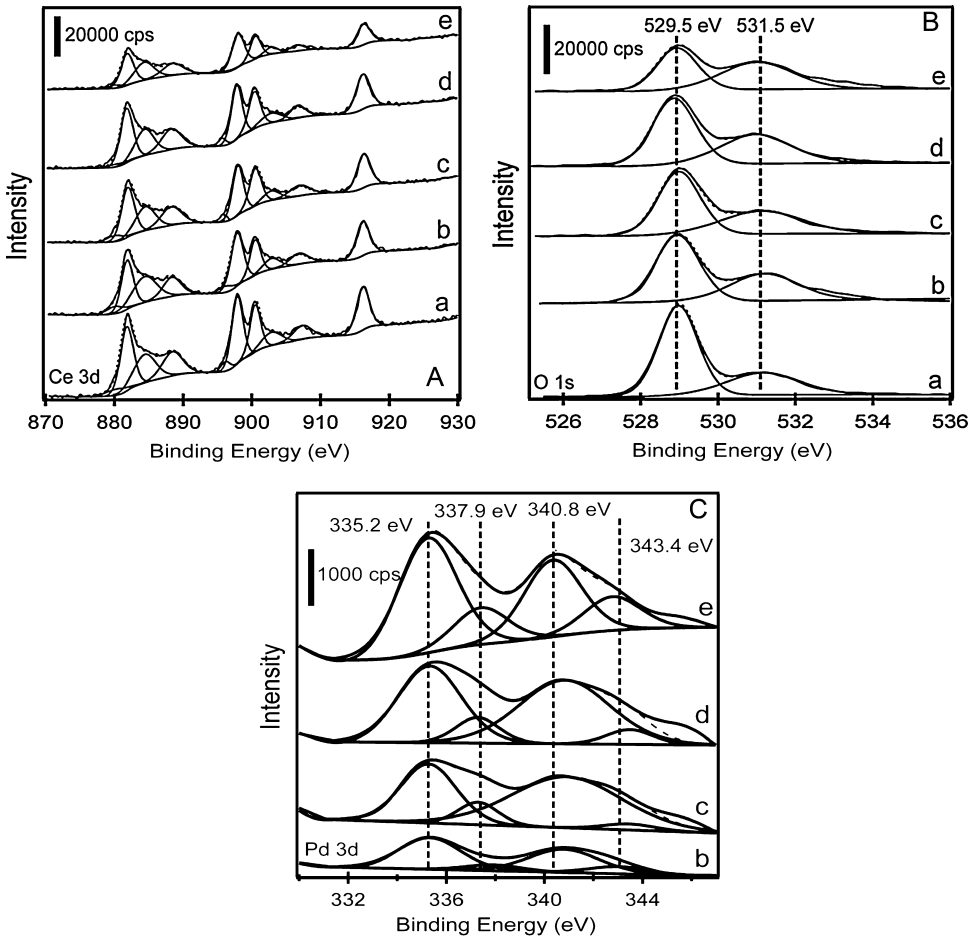

Fig. 5. The XPS spectra of the CeO_2 support (a) and the Pd/CeO_2 catalysts with different Pd loading contents: 1.1 wt% (b), 2.5 wt% (c), 5.1 wt% (d), 9.6 wt% (e).

Table 1
Surface composition of the samples.

Sample	Ce		O		Pd	
	Ce^{3+} (%)	Ce^{4+} (%)	Lattice O (%)	Absorbed O (%)	Pd^0 (%)	Pd^{2+} (%)
1.1 wt% Pd/CeO_2	8.6	10.9	57.3	23.0	0.2	~0.0
2.5 wt% Pd/CeO_2	7.2	12.2	55.0	23.4	1.8	0.4
5.1 wt% Pd/CeO_2	7.0	12.2	46.1	32.7	1.6	0.4
9.6 wt% Pd/CeO_2	6.5	9.1	38.4	42.6	2.8	0.6

Table 2
The assignment of Ce 3d photoelectron peaks of the samples.

Sample	Ce^{3+} $3d_{5/2}$ (eV)		Ce^{4+} $3d_{5/2}$ (eV)			Ce^{3+} $3d_{3/2}$ (eV)		Ce^{4+} $3d_{3/2}$ (eV)		
	υ_0	υ'	υ	υ''	υ'''	u_0	u'	u'	u''	u'''
CeO_2	880.3	884.4	881.8	888.5	896.2	897.9	902.9	900.5	907.4	916.2
1.1 wt% Pd/CeO_2	880.3	884.4	881.9	888.4	896.2	897.9	902.9	900.5	906.9	916.2
2.5 wt% Pd/CeO_2	880.1	884.5	882.0	888.2	896.3	898.0	902.9	900.5	907.0	916.3
5.1 wt% Pd/CeO_2	880.3	884.4	881.8	888.2	895.7	897.8	902.8	900.4	906.7	916.2
9.6 wt% Pd/CeO_2	880.1	884.3	881.9	888.5	895.8	898.0	902.8	900.5	906.6	916.2

increases. Typically, the binding energies of Pd^0 and Pd^{2+} states are 335.2 and 340.8 eV, 337.9 and 343.4 eV, respectively, according to the $3d_{5/2\text{-}3/2}$ spin-orbital doublet [8,11,25–29]. It can be found that most of the Pd element exists as Pd^0 in Pd/CeO_2 catalyst (Table 1). This may be concerned with the synthesized method in the experiment (post-grafting and reduction).

The catalytic performance of mesoporous CeO_2 support and corresponding Pd loaded samples for CO oxidation under dry condition are shown in Fig. 6. The CeO_2 support does not show any catalytic activity when reaction temperature lower than 100 °C. After loaded with palladium, the catalytic activity for CO oxidation shows significant increases. As the Pd loading content increases from 1.1 wt% to 2.5 wt%, the CO total conversion temperature decrease from 90 °C to 40 °C, which is also much lower than that synthesized by other method [11,12]. The corresponding TOFs were derived from the same condition (20 °C) to gain the intrinsic activities of Pd/CeO_2 catalysts. The 2.5 wt% Pd loaded catalyst gives a TOF value of $23.60 \times 10^{-3}\ s^{-1}$, exhibiting significantly higher catalytic activity than that of 1.1 wt% Pd ($6.727 \times 10^{-3}\ s^{-1}$). Further increasing Pd content does not produce additional decrease of the conversion temperature. The catalytic activity of Pd/CeO_2 catalyst is not only determined by the active component (palladium), the geometric structures of CeO_2 support and the synergy between palladium and CeO_2 also play important role for CO oxidation process [14,29,30,31]. Also for 2.5 wt% Pd loaded catalyst at 40 °C, the CO conversion remained almost unchanged over 24 h indicating the high stability under dry condition (Fig. 6B).

Moisture is inevitably existed in practical applications especially at low temperature. Thus, it is more important to study the catalytic behavior of the Pd/CeO_2 catalyst under moisture condition. Surprisingly, when 2.5 vol% H_2O was introduced into the feed gas, the catalytic activity of 2.5 wt% Pd loaded catalyst showed significantly enhancement. The CO total conversion temperature decreases from 40 °C to 30 °C, the TOF value increases from $23.60 \times 10^{-3}\ s^{-1}$ to $38.48 \times 10^{-3}\ s^{-1}$ correspondingly, as shown in Fig. 7. The catalytic stability under moisture condition was also investigated, and the CO conversion gradually decreases from 100% to 75% within 15 h at 40 °C. However, it can be recovered only after dried at 60 °C. What caused the deactivation? After reaction, the deactivated catalyst was characterized by XRD, TEM and N_2 adsorption-desorption measurement, no structure collapse or phase segregation could be observed (Supporting information). The deactivation is unlikely to be due to the physical and textural changes in the catalyst system. It may be attributed to the relatively high moisture concentration, which can lead to H_2O capillary condensation in the smaller pores of the CeO_2 support, consequently preventing the access of the reactants to the catalyst surface. Generally, increasing the temperature can eliminate the phenomenon of H_2O capillary condensation. Just as expected, when reaction temperature raise to 60 °C, the CO conversion remained 100% unchanged even after 24 h reaction.

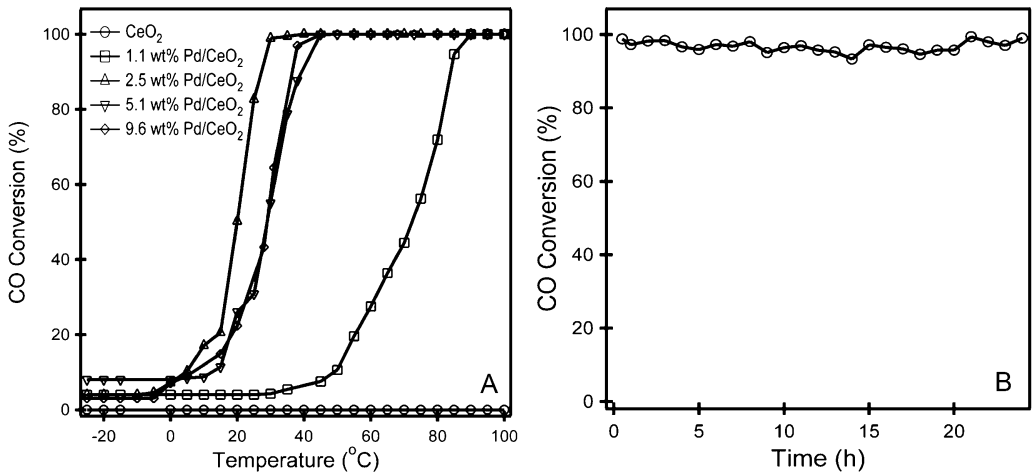

Fig. 6. (A) The catalytic performances of CeO_2 support and Pd/CeO_2 catalysts with different Pd loading contents. (B) The stability of 2.5 wt% Pd loaded catalyst under dry condition at 40 °C.

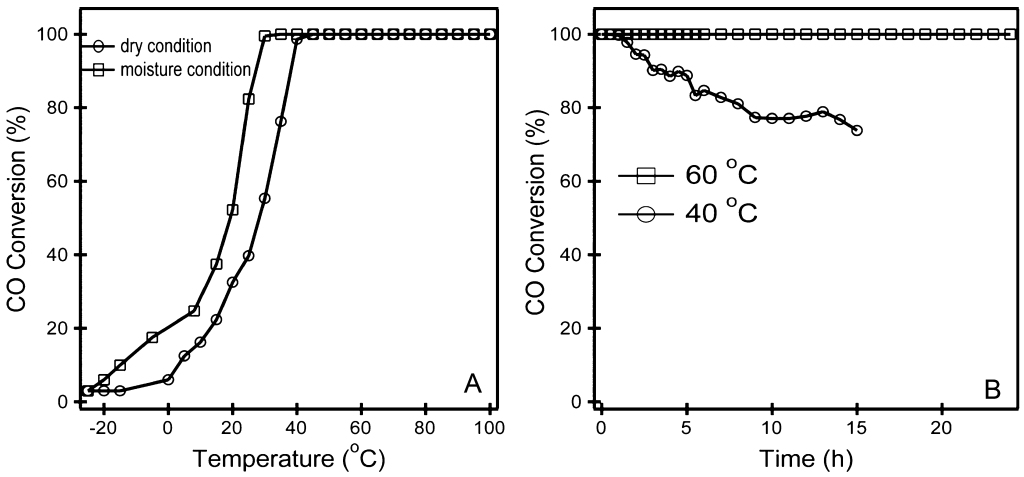

Fig. 7. (A) The catalytic performances of 2.5 wt% Pd loaded catalyst under different reaction conditions. (B) The stability of 2.5 wt% Pd loaded catalyst under moisture condition at different temperatures.

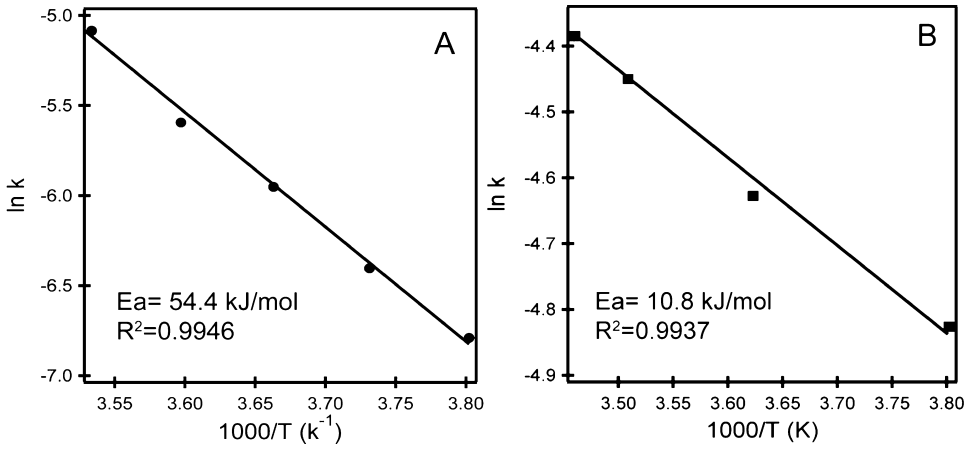

Fig. 8. Arrhenius plots for the reaction rate of CO oxidation (activation energy, E_a) on 2.5 wt% Pd loaded catalyst under dry condition (A) and moisture condition (B).

Besides, water–gas shift reaction was also studied in the experiment to exclude the effect from it. When O_2 was wiped off from the feed gas, the CO conversion can be totally ignored. All these results clearly demonstrate that the presence of water molecules can promote the CO oxidation process when Pd/CeO_2 was used as catalyst.

To further porve the motivation behavior of the H_2O molecules, the apparent activation energies for CO oxidation under different reaction conditions were calculated from the Arrhenius plot, as shown in Fig. 8. The reactions were carried out at differential mode with CO conversions typically less than 15%. The 2.5 wt% Pd loaded catalyst gives a specific reaction rate of 0.018 $mol_{CO}/g_{Pd}/h$ at 25 °C, which is lower than that of 4.4% Au/Fe_2O_3 (0.091 $mol_{CO}/g_{Pd}/h$) [32]. Under dry condition, the apparent activation energy was calculated to be 51.7 kJ mol^{-1}, much higher than that under moisture condition, 10.8 kJ mol^{-1}. It clearly indicates that 2.5 wt% Pd loaded catalyst is an excellent catalyst for low temperature CO oxidation especially under the moisture condition. The presence of water molecules can drastically lower the activation energy and promote the CO oxidation process.

The reaction mechanism of CO oxidation on Pd/CeO_2 catalyst under dry condition has been well established [14–16,30,33]. It was suggested that CeO_2 could supply the lattice O for the CO reaction. The deposition of palladium stimulated the mobility of the oxygen in the CeO_2 lattice. Such an interaction between Pd nanoparticles and the oxide support can be regarded as a kind of synergetic catalytic effect recently proposed [29]. How about that under moisture condition? Based on the fact that the existence of water molecular can promote the CO oxidation process, the proposed synergetic mechanism is shown in Scheme 1. Companied with the process of CO combining with lattice O, the H_2O molecular also reacts with CO forming very reactive absorbed intermediate, $COOH_{(ad)}$, which can be decomposed to CO_2 and H [17,34–37]. Then, the H from H_2O and COOH react with the absorbed O to form H_2O and CO_2.

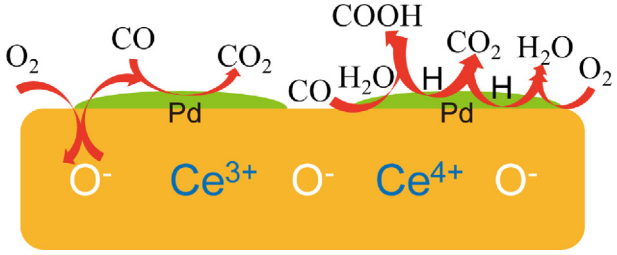

Scheme 1. The possible synergetic mechanism of Pd/CeO_2 catalyst for CO reaction under moisture condition.

4. Conclusion

The Pd/CeO_2 catalyst was successfully prepared by an improved impregnation protocol. The resulting materials possessed relatively high specific surface area and highly dispersed Pd nanoparticles. For low temperature CO oxidation reaction, 2.5 wt% Pd loaded catalyst showed the much higher reaction activity. The total conversion temperature was as low as 40 °C under dry condition. When 2.5 vol% H_2O was introduced into the feed gas, the catalytic activity showed significantly enhancement. The CO total conversion temperature decreased from 40 °C to 30 °C. The presence of water molecular could promote the CO oxidation process due to the relative lower apparent activation energy.

Acknowledgement

This study was supported by National Basic Research Program of China 2013CB933201.

Appendix A. Supplementary data

Supplementary data associated with this article can be found, in the online version, at http://dx.doi.org/10.1016/j.apcatb.2014.04.030.

References

[1] E.L. Crepaldi, G.J. de, A.A. Soler-Illia, A. Bouchara, D. Grosso, D. Durand, C. Sanchez, Angew. Chem. Int. Ed. 42 (2003) 347–351.
[2] K.-i. Fujimoto, F.H. Ribeiro, M. Avalos-Borja, E. Iglesia, J. Catal. 179 (1998) 431–442.
[3] P.O. Thevenin, A. Alcalde, L.J. Pettersson, S.G. Järås, J.L.G. Fierro, J. Catal. 215 (2003) 78–86.
[4] W.F. Libby, Science 171 (1971) 499–500.
[5] J.-Y. Luo, M. Meng, J.-S. Yao, X.-G. Li, Y.-Q. Zha, X. Wang, T.-Y. Zhang, Appl. Catal. B: Environ. 87 (2009) 92–103.
[6] S. Colussi, A. Gayen, M.F. Camellone, M. Boaro, J. Llorca, S. Fabris, A. Trovarelli, Angew. Chem. Int. Ed. 48 (2009) 8481–8484.
[7] K.R. Priolkar, P. Bera, P.R. Sarode, M.S. Hegde, S. Emura, R. Kumashiro, N.P. Lalla, Chem. Mater. 14 (2002) 2120–2128.
[8] P. Bera, K.C. Patil, V. Jayaram, G.N. Subbanna, M.S. Hegde, J. Catal. 196 (2000) 293–301.
[9] D.B. Meadowcroft, Nature 226 (1970) 847–848.
[10] R.V. Gulyaev, E.M. Slavinskaya, S.A. Novopashin, D.V. Smovzh, A.V. Zaikovskii, D.Yu. Osadchii, O.A. Bulavchenko, S.V. Korenev, A.I. Boronin, Appl. Catal. B: Environ. 147 (2014) 132–143.
[11] B. Wang, D. Weng, X. Wu, R. Ran, Appl. Surf. Sci. 257 (2011) 3878–3883.
[12] A.K. Datye, J. Bravo, T.R. Nelson, P. Atanasova, M. Lyubovsky, L. Pfefferle, Appl. Catal. A: Gen. 198 (2000) 179–196.
[13] A.S. Ivanova, E.M. Slavinskaya, R.V. Gulyaev, V.I. Zaikovskii, O.A. Stonkus, I.G. Danilova, L.M. Plyasova, I.A. Polukhina, A.I. Boronin, Appl. Catal. B: Environ. 97 (2010) 57–71.
[14] M.S. Hegde, G. Madras, K.C. Patil, Accounts Chem. Res. 42 (2009) 704–712.
[15] H. He, H.X. Dai, C.T. Au, Catal. Today 90 (2004) 245–254.
[16] G. Li, Q. Wang, B. Zhao, R. Zhou, Catal. Today 158 (2010) 385–392.
[17] J. Bergeld, B. Kasemo, D.V. Chakarov, Surf. Sci. 495 (2001) L815–L820.
[18] H.-F. Wang, R. Kavanagh, Y.-L. Guo, Y. Guo, G.-Z. Lu, P. Hu, Angew. Chem. Int. Ed. 51 (2012) 6657–6661.
[19] X.W. Xie, L. Li, Z.-Q. Liu, M. Haruta, W.J. Shen, Nature 458 (2009) 746–749.
[20] M. Dat, M. Okumura, S. Tsubota, M. Haruta, Angew. Chem. Int. Ed. 43 (2004) 2129–2132.
[21] C.C. Yu, L.X. Zhang, J.L. Shi, J.J. Zhao, J.H. Gao, D.S. Yan, Adv. Funct. Mater. 18 (2008) 1544–1554.
[22] Y.J. Feng, L. Li, S.F. Niu, Y. Qu, Q. Zhang, Y.S. Li, W.R. Zhao, H. Li, J.L. Shi, Appl. Cata. B: Environ. 111 (2012) 461–466.
[23] M. Passacantando, S. Santucci, J. Nanopart. Res. 15 (2013) 1785.
[24] F. Morales, D. Grandjean, A. Mens, F.M.F. de Groot, B.M. Weckhuysen, J. Phys. Chem. B 110 (2006) 8626–8639.
[25] Z. Gao, Y. Feng, F. Cui, Z. Hua, J. Zhou, Y. Zhu, J. Shi, J. Mol. Catal. A: Chem. 336 (2011) 51–57.
[26] M.B. Bellakki, T. Baidya, C. Shivakumara, et al., Appl. Catal. B: Environ. 84 (2008) 474–481.
[27] S. Roy, A. Marimuthu, M.S. Hedge, G. Madras, Appl. Catal. B: Environ. 71 (2007) 23–31.
[28] P.A. Deshpande, M.S. Hedge, G. Madras, Appl. Catal. B: Environ. 96 (2010) 83–93.
[29] R.V. Gulyaev, A.I. Stadnichenko, E.M. Slavinskaya, A.S. Ivanova, S.V. Koscheev, A.I. Boronin, Appl. Catal. A: Gen. 439–440 (2010) 41–50.
[30] A. Trovarelli, Catal. Rev.-Sci. Eng. 38 (1996) 439–520.
[31] J.L. Shi, Chem. Rev. 113 (2013) 2139–2181.
[32] J.S. Lee, S.H. Choi, K.D. Kim, M. Nomura, Appl. Catal. B: Environ. 7 (1996) 199–212.
[33] A.I. Boronin, E.M. Slavinskaya, I.G. Danilova, R.V. Gulyaev, Y.I. Amosov, P.A. Kuznetsov, I.A. Polukhina, S.V. Koscheev, V.I. Zaikovskii, A.S. Noskov, Catal. Today 144 (2009) 201–211.
[34] T. Schalow, M. Laurin, B. Brandt, S. Schauermann, S. Guimond, H. Kuhlenbeck, D.E. Starr, S.K. Shaikhutdinov, J. Libuda, H.J. Freund, Angew. Chem. Int. Ed. 45 (2006) 7601.
[35] S. Golunski, R. Rajaram, N. Hodge, G.J. Hutchings, J.C. Kiely, Catal. Today 72 (2002) 107.
[36] O. Pozdnyakova, D. Teschner, A. Wootsch, J. Kröhnert, B. Steinhauer, H. Sauer, L. Toth, F.C. Jentoft, A. Knop-Gericke, Z. Paál, J. Catal. 237 (2006) 17–28.
[37] B. Qiao, L. Liu, J. Zhang, Y. Deng, J. Catal. 261 (2009) 241–244.